Knight shift of n type indium antimonide near the quantum limit*

Gilbert A. Miranda,†‡John A. McNeil,§and W. Gilbert Clark
Department of Physics, University of California, Los Angeles, California 90024
(Received 21 May 1973)

Measurements of the Knight shift in n-type InSb at low temperatures (0.4–4.2 K) are presented as a function of magnetic field H_0 near the quantum limit for several conduction-electron concentrations (2×10^{14}–1.2×10^{16} cm^{-3}). The observed shift is separated into the chemical shift and the hyperfine shift (ΔH). The hyperfine shift exhibits quantum oscillations (QO) as the field is varied. As with the de Haas–van Alphen effect and the QO of the nuclear spin-lattice relaxation rate ($1/T_1$), they are caused by oscillations in the conduction-electron density of states at the Fermi energy which occur as the magnetic field is changed. These experiments indicate that the density of states is broadened. This broadening is caused by either or both of two mechanisms: electron collisions with charged impurities (Dingle broadening) and the random spatial fluctuations in the impurity density (band tailing). Theoretical calculation of ΔH vs H_0 are presented and the numerical solutions are given. In these calculations, Dingle broadening is approximated as an added increment of temperature (the Dingle temperature T_D). The theory of Dyakonov, Efros, and Mitchell is used to calculate the effects of band tailing. The differences between ΔH-vs-H_0 curves calculated on the basis of each mechanism are small and are not observable in InSb. No variations in Δ-H were observed at fields which correspond to the type-A and type-B peaks observed in $1/T_1$ by Bridges and Clark.

I. INTRODUCTION

The properties of n-type InSb are such that, in easily obtained magnetic fields, all the electrons are in the last few Landau subbands ($l = 0$–4). In this range of fields, the electrons are approaching the quantum limit $\hbar\omega_c \gtrsim \mu$ ($\omega_c = eH/m^*c$ is the cyclotron frequency and μ is the Fermi energy). Under these conditions there will be large quantum oscillations (QO) in the electronic density of states at the Fermi energy and, consequently, in phenomena which depend on it. One of these phenomena is the Knight shift, which is the subject of this research. Other types of QO which have been reported in InSb are the de Haas–van Alphen effect,[1] the Shubnikov–de Haas effect,[2–4] QO in the nuclear spin-lattice relaxation rate ($1/T_1$),[5] and QO in the interband Faraday rotation.[6]

Quantum oscillations of the Knight shift have already been described theoretically for metals and observed experimentally in tin, aluminum, and cadmium.[7–17] These calculations and measurements have all been performed far away from the quantum limit, i.e., for fields such that $\hbar\omega_c \ll \mu$. Unfortunately, there appears to be some confusion among the theoretical workers as to whether or not the QO in the Knight shift can be fully explained by oscillations of the density of states. For this reason it is important to observe the QO near the quantum limit where the shifts can be calculated explicitly and compared unambiguously to the experimental results. This is the case in the present work on InSb.

The experimental work reported here includes measurements of the Knight shift in single-crystal InSb from 4.2 to 0.4 K as a function of magnetic field from 4 to 20 kOe for several values of conduction-electron concentration n_0 (2×10^{14} to 1.2×10^{16} cm^{-3}). In addition to the experimental work, calculations and numerical solutions describing the QO are given.

There is some overlap between our work and the recent work of Willig and Sapoval,[18] which was done simultaneously and independently. Except for some minor differences in experimentally measured numbers, both works are in substantial agreement. The origin of the small discrepancies is not clear at this time, and probably unimportant in terms of physical consequences. The work reported here covers a wider range of variables, has a greater experimental accuracy, and a more detailed analysis in comparison with that of Willig and Sapoval.

In InSb there are three contributions to the relative shift: (i) the chemical shift,[19] which is expected to be independent of field, temperature, and electron concentration for the ranges of these variables encountered here; (ii) the hyperfine shift ΔH, due to the contact hyperfine interaction[20] with s electrons; and (iii) the orbital contribution to the hyperfine shift. Since the latter is expected to be only about 4×10^{-3} of the contact interaction,[21] it will not be considered further in this work. The quantity of interest in this paper is the hyperfine shift. In our measurements it was found that the density of states is a smoother function of energy than that expected of a uniform density of free electrons in a perfect lattice. Therefore, two mechanisms for nonthermal broadening of the density of states are included in the calculations. The first is a broadening of the electronic eigenstates

due to collisions with charged impurities[22] (Dingle broadening). The second mechanism is the spatial fluctuations in the electronic potential energy due to the random distribution of donor ions in the crystal[23] (band tailing).

The major experimental results of this work are the observation of QO of the hyperfine shift in InSb near the quantum limit. The positions, shapes, and amplitudes of the QO are found to agree with the calculated results when either of the broadening mechanisms are included. Unfortunately, it is not possible with our data to assess the relative importance of these two mechanisms since the results of their application, separately or in combination, are indistinguishable within our experimental resolution. In addition, there were no apparent changes in ΔH found which would correspond to the type-A or type-B peaks in $1/T_1$ observed by Bridges and Clark[5] (hereafter referred to as BC).

The organization of this paper is as follows. In Sec. II the samples, apparatus, and experimental methods are presented. Section III is devoted to the experimental results. In Sec. IV our interpretation of the experimental results is given, including calculations of the quantum oscillations in ΔH. The conclusions are stated in Sec. V.

II. EXPERIMENTAL DETAILS

A. Samples

The InSb samples used in this experiment are the same neutron-irradiation-doped single crystals used in previous experiments by other workers.[3,5,24-26] Their properties are listed in Table I. The three samples to be discussed are identified by the letters A, B, and C; their nominal concentrations are 2.04×10^{14}, 3.34×10^{15}, and 1.18×10^{16} cm^{-3}, respectively.[26] It should be noted that the actual concentration of conduction electrons is dependent on the temperature and the magnetic field and may be different from the nominal concentration. As pointed out by BC, the values of n_0 are obtained from Hall-effect measurements in the limit where the magnetic field and the measuring current become very small. These values of n_0 are constant to within 3% from 1.3 to 77 K. They further point out that in this temperature range for magnetic fields less than 20 kOe the concentration remains constant for samples with $n_0 \gtrsim 10^{15}$ cm^{-3} and tends to decrease with decreasing T for samples with lower n_0. This decrease is due to magnetic freeze-out, which has been discussed in detail by other authors.[4,27-34]

All samples were mounted with the external field applied in the [001] direction and the NMR coil axis in the [$\bar{1}$10] direction. This orientation was chosen to maximize the nuclear spin-lattice relaxation rates.[5]

B. Measurements

The experimental quantities to be measured in this experiment were the nuclear resonance frequencies of the In^{115} and Br^{79} nuclei (ν_{115} and ν_{79}) in the same magnetic field, and the temperature. The bromine resonance was used as a reference with which to compare the indium resonance frequency.

Severe difficulties were encountered in obtaining the resonance measurements for these experiments. We will simply indicate their nature here. The detailed solutions to these problems are discussed elsewhere.[35] First, although the In^{115} lines are broad (~ 9 Oe), physically meaningful results required locating the center of the line to about ± 0.15 Oe or ± 1.7% of the linewidth. This problem was compounded for the In^{115} resonance, as the 4% abundant isotope In^{113} has its resonance very close to that of In^{115}, thereby producing a slightly asymmetric absorption line. A second major problem was that the nuclear spin-lattice relaxation times

TABLE I. Sample properties.

Sample	n_0[a] (10^{15} cm^{-3})	$\left(\frac{m^*}{m_e}\right)$[b]	g^*[c]	Cyclotron splitting at 1 kOe[d] $\frac{\hbar\omega_c}{k}$ (K)	Spin splitting at 1 kOe[d] $\frac{\hbar\omega_e}{k}$ (K)	$\beta=\left(\frac{\omega_c}{\omega_e}\right)$[d]	Fermi energy (μ) at T, $H=0$[e] (K)
A	0.204	0.013	−51.1	10.51	3.43	3.06	11.5
B	3.34	0.014	−48.6	9.35	3.27	2.86	61.7
C	11.8	0.016	−45.0	8.27	3.03	2.73	135

[a]Reference 26.
[b]C. Hilsum and A. C. Rose-Innes, *Semiconducting III-V Compounds* (Pergamon, New York, 1961), p. 43.
[c]Reference 24.
[d]Calculated from g^* and m^*.
[e]Calculated from free-electron theory using m^* and n_0.

for the InSb were in the range 2–40 h. This made it necessary to use very low levels of rf excitation to avoid excessive saturation of the line.

The temperatures used in this experiment were 0.4, 1.5, and 4.2 K. They were produced by immersing the sample and NMR coils in pumped, liquid He^3 or He^4. Temperatures were monitored by measuring the vapor pressure over the liquid.

The quantity of interest in this work is the hyperfine field shift (ΔH) of the nuclear resonance in InSb due to the conduction electrons. The experimentally observed relative shift (K) is measured using a dilute solution of the appropriate compound as a reference. This observed shift is a combination of both the hyperfine shift and the chemical shift of InSb. The chemical shift is expected to be independent of impurity concentration, magnetic field, and temperature over the ranges of these variables covered here.[19] Although the observed shift is a mixture of hyperfine and chemical shifts, it is fortunately possible in the work presented here to obtain separately the hyperfine shift by making measurements at several difference values of n_0 as explained in Sec. III.

The experimental values of K were obtained by measuring the nuclear resonance frequency of the appropriate nucleus in InSb and that of the Br^{79} in the same magnetic field. The ratio of these frequencies was taken and compared with the ratio similarly determined for the appropriate reference sample. There are three species of abundant nuclei in InSb: In^{115}, Sb^{121}, and Sb^{123}. Since the In^{115} resonance offers much more sensitivity than the others, almost all of our measurements were made on it. In addition, a few measurements were made on Sb^{121}. In the case of In^{115}, the reference sample was a dilute $In_2(SO_4)_3$ solution, for Sb^{121} it was dilute $HSbF_6$.[36] The Br^{79} resonance was obtained from several pieces of KBr single crystal surrounding the InSb crystal.

Most of the data were taken using steady-state NMR absorption techniques. The accuracy of these measurements is typically ± 0.15 Oe for In^{115} and ± 0.4 Oe for Sb^{121}. A few measurements were obtained with pulsed NMR methods. Their accuracy was about ± 0.2 Oe for In^{115} above 12 kOe.

The accuracies of (ν_{115}/ν_{79}) and (ν_{121}/ν_{79}) for the reference compounds [$In_2(SO_4)_3$ and $HSbF_6$] are $\pm 0.0005\%$ and $\pm 0.0027\%$, respectively. These errors are equivalent to an uncertainty in the location of the $K=0$ point for the respective measurements on InSb. Thus, if a more accurate reference measurement becomes available, this extra uncertainty in K can be reduced.

One other possible source of error in the measurements of K as they appear here is the change in the chemical shift of Br^{79} in KBr single crystal as the temperature is reduced from room temperature to liquid-helium temperature. This temperature dependence of the Br^{79} chemical shift has not, to our knowledge, been investigated, but its effect can be estimated from the available data for KI crystals.[37] Based on these data we estimate that this effect may cause our quoted value of K to be too low by 0.0006–0.0016%.

In the analysis of the data to obtain the hyperfine shift from the measured K values, it will be shown that each of the aforementioned errors in the reference drop out exactly.

The magentic field dependence of K was measured from 4 to 20 kOe. Below 4 kOe, the signals were too weak to give reasonable accuracies, thus the measurements presented here have been restricted to magnetic fields above 4 kOe, and in some cases higher.

III. EXPERIMENTAL RESULTS

The phenomenon of interest in this experiment is the dependence of the NMR hyperfine field shift (ΔH) on the magnetic field (H_0), the electronic concentration (n_0), and the temperature (T). The experimentally observed field shift (KH_0) measured with respect to $In_2(SO_4)_3$, however, is the sum of this hyperfine field shift and the chemical field shift (σH_0). In terms of relative shifts

$$K = \Delta H/H_0 - \sigma, \tag{1}$$

where the sign of σ is such that a diamagnetic shift is positive. Using the experimental data for samples A and C, it is possible to separate these two contributions to the hyperfine field shift. For magnetic fields exceeding 1.87 kOe, the conduction electrons in sample A will be completely polarized into the lower spin state. The hyperfine field shift is then maximum, and is independent of magnetic field and temperature, and is proportional to the electron concentration in this sample ($\Delta H_A = h n_{0A}$). The factor (h) is the hyperfine field shift per unit conduction-electron concentration, and is assumed to be characteristic of n-type InSb, and independent of sample concentration. The chemical shift (σ) is also assumed to be sample, field, and temperature independent.

By rearranging Eq. (1) and averaging over experimental points for sample A, we get for σ,

$$\sigma = (h n_{0A} - \langle K_A H_A \rangle)/\langle H_A \rangle . \tag{2}$$

Similarly, using values of K and H_0 for sample C in Eq. (1), and combining the results with Eq. (2), we get for h

$$h = (K_C \langle H_A \rangle - \langle K_A H_A \rangle)(\Delta n_C \langle H_A \rangle / H_C - n_{0A})^{-1} . \tag{3}$$

After substituting the theoretical value 3.93×10^{15} cm^{-3} for Δn_C at $H_C = 19$ kOe and using smoothed data for In^{115} for sample C, we obtain for h,

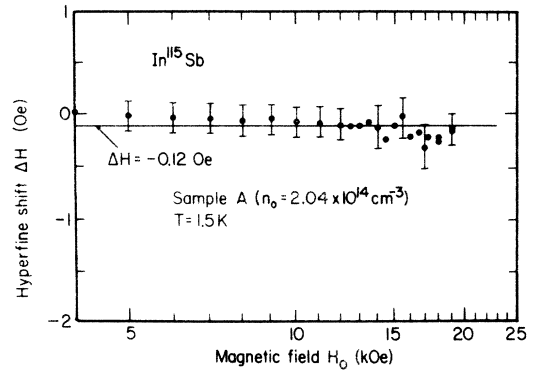

FIG. 1. Experimental hyperfine resonance shift for n-type $In^{115}Sb$ in sample A($n_0 = 2.04 \times 10^{14}$ cm^{-3}) as a function of magnetic field for $T = 1.5$ K. Within experimental resolution the data lie on the straight line $\Delta H = -0.12$ Oe.

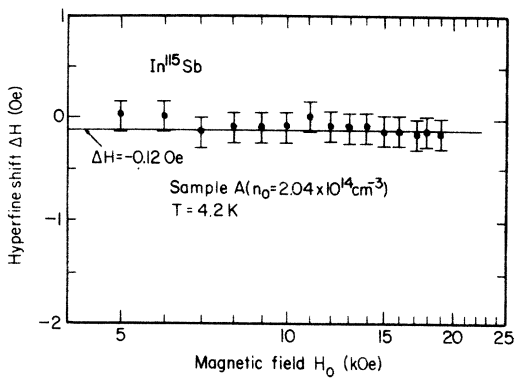

FIG. 2. Experimental hyperfine shift for n-type $In^{115}Sb$ in sample A($n_0 = 2.04 \times 10^{14}$ cm^{-3}) as a function of magnetic field for $T = 4.2$ K. As with the data at 1.5 K (Fig. 1), these lie on the line $\Delta H = -0.12$ Oe. QO for this concentration occur below 2 kOe.

$$h^{115}_{\text{expt}} = -(0.589 \pm 0.050) \times 10^{-15} \text{ Oe cm}^3, \quad (4)$$

and for σ, using Eq. (2)

$$\sigma_{115} = -(0.0091 \pm 0.0008)\%. \quad (5)$$

With these results the values of ΔH can be obtained directly from Eq. (1). It can be seen by examining Eqs. (1)–(3) that the errors in locating the $K = 0$ point cancel exactly in the expression for ΔH.

A. Sample A

Figure 1 shows measurements of ΔH for In^{115} as a function of H_0 for $T = 1.5$ K in sample A ($n_0 = 2.04 \times 10^{14}$ cm^{-3}). Within experimental error, the data lie on a straight horizontal line at $\Delta H = -0.12$ Oe over the entire range of magnetic field. Figure 2 shows similar measurements for $T = 4.2$ K. These data lie on the same straight line indicated for the data at 1.5 K. Data for Sb^{121} at 1.5 K (not shown) also follow a straight horizontal line within experimental error. This field-independent shift above 4 kOe is as expected for the low electron concentration in this sample.

B. Sample B

Measurements of ΔH for In^{115} at 1.5 and 4.2 K in sample B ($n_0 = 3.34 \times 10^{15}$ cm^{-3}) are shown in Figs. 3 and 4, respectively. Between 4 and 7 kOe, ΔH decreases with increasing H_0, dropping more rapidly above 7 kOe. The data at 4.2 K become saturated at $\Delta H = -1.97 \pm 0.11$ Oe for fields above 13.5 kOe. For purposes of identification this saturated region will be referred to as the 0, − region. It is worth noting that these data deviate significantly from proportionality to H_0, which characterizes the normal behavior of the hyperfine shift. The curves calculated from theory have been included for comparison. The scatter for the Sb^{121} data is sufficiently large that all interesting features are obliterated, and these data are thus not shown.

C. Sample C

Quantum oscillations are clearly visible in the hyperfine shift data for sample C ($n_0 = 1.18 \times 10^{16}$ cm^{-3}) presented in Figs. 5 and 6 for $T = 1.5$ and 0.4 K, respectively. ΔH drops with field to a minimum at about 11 kOe, and rises to a maximum around 14 kOe. Beyond 14 kOe the shift drops off rapidly to what is probably a saturated region similar to that of sample B at 4.2 K. For purposes of comparison with theory, the minimum near 11 kOe will be called the 1, + dip and the maximum near 14 kOe will be called the 1, − peak. Calculated curves have been included for compari-

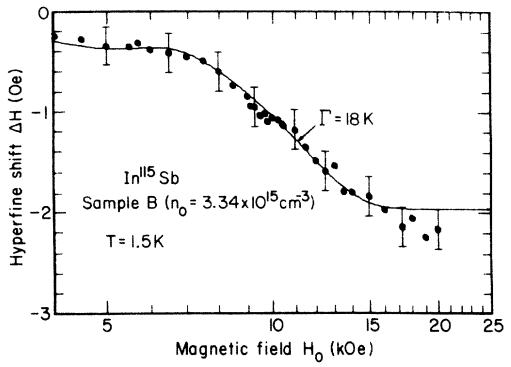

FIG. 3. Experimental hyperfine shift for n-type $In^{115}Sb$ at 1.5 K in sample B ($n_0 = 3.34 \times 10^{15}$ cm^{-3}) as a function of magnetic field. Above 15 kOe complete polarization of the conduction electron spins is observed. The solid curve is the best fit calculated from the theory using band tailing with $\Gamma = 18$ K.

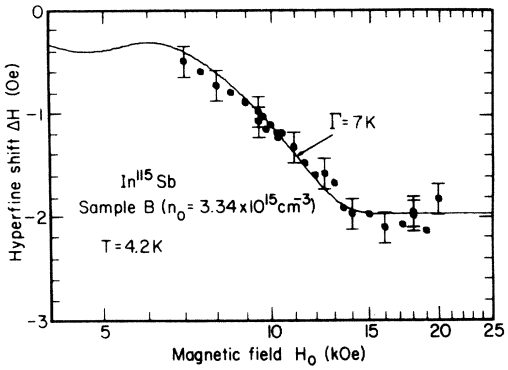

FIG. 4. Experimental hyperfine shift for n-type $In^{115}Sb$ as a function of magnetic field for sample B ($n_0 = 3.34 \times 10^{15}$ cm^{-3}) at $T = 4.2$ K. Above 13.5 kOe the shift becomes saturated at $\Delta H = -1.97 \pm 0.11$ Oe. In this region, the 0,+ Landau subband has become completely depopulated and all electrons are in the 0, − subband. The curve is the best fit calculated from the band-tailing theory with $\Gamma = 7$ K.

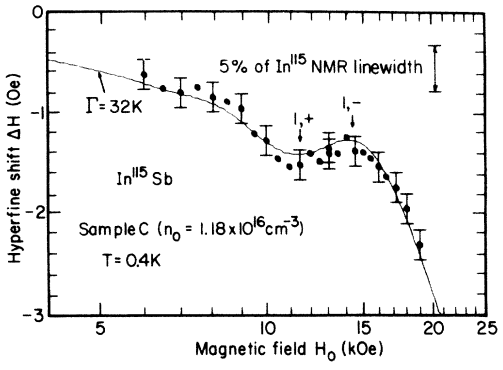

FIG. 6. Experimental hyperfine shift for n-type $In^{115}Sb$ as a function of magnetic field for sample C ($n_0 = 1.18 \times 10^{16}$ cm^{-3}) at 0.4 K. Within experimental resolution these data lie on the same curve as the data for 1.5 K. Beyond 14 kOe the magnitude of the shift increases rapidly. Saturation of ΔH is expected at still higher fields.

son with theory.

At this point the main features of the data are summarized.

(i) The following are seen as n_0 increases: (a) The number of observed oscillations increases: (b) the field at which a given peak or dip occurs becomes greater; and (c) the amplitude of the oscillations increase.

(ii) The results for samples A and C are independent of temperature.

(iii) Within experimental error, the results for sample B are the same for 1.5 and 4.2 K. However, the data for 1.5 K do suggest that the hyperfine shift might not, in fact, saturate for $H_0 > 16$ kOe (this is the same field at which BC observed a large peak in the nuclear spin-lattice relaxation rate).

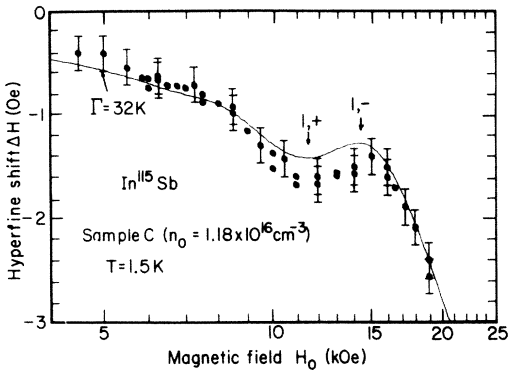

FIG. 5. Experimental hyperfine shift for n-type $In^{115}Sb$ as a function of magnetic field at 1.5 K for sample C ($n_0 = 1.18 \times 10^{16}$ cm^{-3}). QO are clearly visible near 11 and 14 kOe. These correspond to the 1, + and 1, − oscillations, respectively. The curve is the best fit calculated from the band-tailing theory with $\Gamma = 32$ K.

(iv) Below some value of H_0 for samples B and C, ΔH varies smoothly with H_0 and is approximately proportional to it.

(v) The hyperfine shift in sample A is not visibly affected by the mechanism which causes a peak in $1/T_1$, observed previously in this sample[5] (nor is it expected to be).

IV. INTERPRETATION

In this section the hyperfine shift of the nuclear magnetic resonance due to the presence of conduction electrons in n-type InSb is discussed. Also discussed is the broadening or "damping" of the oscillations due to electron collisions and band tailing.

A. Hyperfine resonance shift

In order to aid in visualizing the origin of the QO, the derivation of the hyperfine shift will first be described. Yafet[38] has derived the hyperfine interaction for the case where the electronic g factor is large and has pointed out that, although g^* is used to determine the electron spin splitting in a magnetic field, the free-electron g factor must be used in calculating the contact hyperfine interaction. Gueron has estimated that the orbital contribution to the shift is about 4×10^{-3} of that of the contact interaction with s electrons.[21] The only significant contribution to the hyperfine shift in InSb then comes from the contact hyperfine interaction and all other contributions will be ignored.

The hyperfine shift (ΔH) is proportional to the

difference (Δn) in the populations of electrons with spin parallel and spin antiparallel to the direction of quantization. At magnetic fields high enough that level quantization becomes important ($\hbar\omega > kT$), Δn, and therefore ΔH, become oscillatory functions of H_0. These QO's have been described theoretically for metals by several authors[7-14] and have been observed experimentally for tin, aluminum, and cadmium.[15-18] A prominent feature of the systems investigated previously is that the cyclotron energy is much less than the Fermi energy ($\hbar\omega_c \ll \mu$). This is in contrast to InSb where $\hbar\omega_c \sim \mu$ at reasonably low magnetic fields (4–20 kOe for the samples used here).

In order to facilitate comparison of the experimental results with theoretical predictions, a brief summary of the theory will be given here.[39] BC have given a review of the calculation of the nuclear spin-lattice relaxation rate oscillations for nonzero temperatures in the case where $\mu \lesssim \hbar\omega_c$. Our discussion will be phrased in terms similar to theirs.

In this calculation we use free-electron theory with the effective-mass approximation in which the electrons have an effective mass m^* ($\simeq 0.013$ free-electron mass) and an effective g factor ($g^* \simeq -50$). The Fermi surface of InSb is very nearly spherical. In the range of impurity concentrations covered here the conduction band is approximately parabolic.[40]

We shall ignore any changes in the effective mass and a g factor with electron kinetic energy,[24,41-43] temperature,[44,45] and applied magnetic field,[46-48] since they are small for the ranges of variables considered here.

The Hamiltonian for the contact hyperfine interaction between the electron and nucleus is

$$H' = \tfrac{8}{3}\pi \gamma_e \gamma_n \hbar^2 \vec{I} \cdot \vec{S}\, \delta(\vec{r}), \tag{6}$$

where γ_e is the free-electron gyromagnetic ratio, γ_n that for the nucleus, and $\vec{r}$ is the electron's position relative to the nucleus. With the magnetic field applied in the z direction and assuming the spatial part of the electron wave function to be independent of spin and wave vector,[49] the interaction is integrated over electron states and averaged over a thermal distribution of electrons. This gives the usual expression for the resonance shift:

$$\Delta H = \pm \tfrac{8}{3}\pi \langle |u_F(0)|^2 \rangle \Omega \mu_B \Delta n, \tag{7a}$$

$$\Delta n = n_- - n_+ , \tag{7b}$$

$$n_\pm = \int f(E) g_\pm(E)\, dE, \tag{7c}$$

where the sign is taken to be the same as that of g^*. The quantity Δn is defined here to always be positive, $\langle |u_F(0)|^2 \rangle$ is the squared Bloch function amplitude at the nucleus averaged on the Fermi surface, Ω is the volume of the unit cell, μ_B is the Bohr magneton, $f(E)$ is the Fermi-Dirac distribution function, and $g_\pm(E)$ is the density of states per unit volume and energy for electrons in each spin state. The upper sign refers to the spin state with higher energy and vice versa (in InSb the conduction-electron g factor is negative, and the state with spin parallel to the field is the lower state; this is the reverse of the free-electron case).

The energy levels of a conduction electron in an applied magnetic field are

$$\mathcal{E}_{l,\pm,k_z} = (l + \tfrac{1}{2})\hbar\omega_c + (\hbar k_z)^2/2m^* \pm \tfrac{1}{2}\hbar\omega_e$$
$$= E_{l,\pm,k_z} + \tfrac{1}{2}\hbar\omega_c , \tag{8}$$

where, l, $\pm$ indicate the respective Landau and spin quantum numbers, $\omega_c = eH/m^*c$ is the cyclotron frequency, k_z is the wave vector for motion along the z direction, and $\hbar\omega_e = g^*\mu_B H$ is the electron spin splitting. $E_{l,\pm,k_z}$ is introduced to eliminate the term $\frac{1}{2}\hbar\omega_c$.

Since the motion of conduction electrons along the z direction is unaffected by the presence of the magnetic field, the number of allowed k_z values per unit energy range (g_z) is proportional to $\epsilon_z^{-1/2}$ (ϵ_z is the kinetic energy associated with k_z). When g_z is multiplied by the degeneracy of the Landau level, the density of states per unit volume and energy for a given spin and Landau subband becomes (we drop the subscripts on E and make it an independent variable)

$$g_{l,\pm}(E) = AH(E - l\hbar\omega_c \mp \tfrac{1}{2}\hbar\omega_e)^{-1/2}$$
$$E - l\hbar\omega_c \mp \tfrac{1}{2}\hbar\omega_e \geq 0$$
$$= 0, \quad E - l\hbar\omega_c \mp \tfrac{1}{2}\hbar\omega_e < 0 , \tag{9a}$$

where

$$A = em^{*1/2}/2\sqrt{2}\,\pi^2\hbar^2 c . \tag{9b}$$

The total density of states is obtained by summing over l:

$$g_\pm(E) = \sum_{l=0}^{\infty} g_{l,\pm}(E) . \tag{10}$$

This function is shown for InSb in Fig. 7 from BC. The figure corresponds to an applied field of 10 kOe, $T = 2$ K, and $n_0 = 10^{16}$ cm^{-3}.

It can be seen from the figure that as the applied field is increased, the Landau subbands rise, and one by one pass through the Fermi level. Thus Δn oscillates with increasing field until the 0, + level is reached ($\mu = \frac{1}{2}\hbar\omega_e$) where all electrons become polarized in the same direction ($\Delta n = n_0$). Since all electrons are in the 0, − subband for this region of magnetic field, this will be called the 0, − region. The extrema of the oscillations occur when $\mu \simeq l\hbar\omega_c \pm \frac{1}{2}\hbar\omega_e$ and will be called the l, $\pm$ peaks and dips.

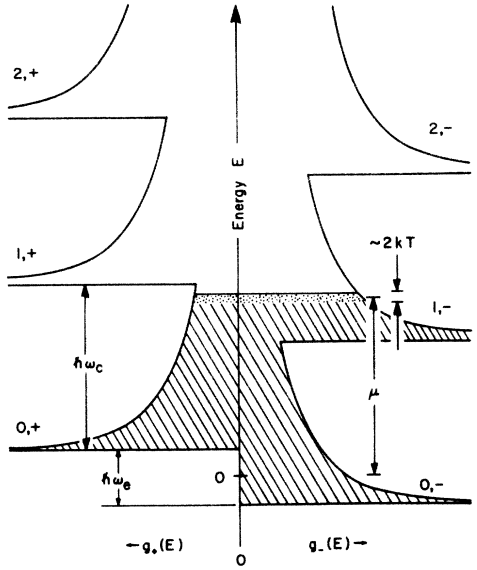

FIG. 7. Conduction-electron density of states in n-type InSb. The figure is drawn for a sample with $n_0 \simeq 10^{16}$ cm^{-3} at a field $H_0 = 10$ kOe with $T = 2$ K. The cross-hatched area represents filled states and the clear area represents empty states. The speckled area is the region of partially occupied states of width $\sim 2kT$ around the Fermi level. Landau subbands up to $l = 2$ are shown here. This figure is reproduced from Ref. 5.

1. Zero temperature

The integral in Eq. (7c) can be evaluated explicitly for $T = 0$ by using Eqs. (9) and (10):

$$n_\pm = (H/H_{0,+})^{3/2} \sum_l (\mu/\hbar\omega_e - l\beta \mp \tfrac{1}{2})^{1/2}, \tag{11a}$$

$$H_{0,+} = [n_0/2A(|g^*|\mu_B)^{1/2}]^{2/3} = (2\pi)^{1/3}(\pi\hbar c/e)n_0^{2/3}\beta^{1/3}, \tag{11b}$$

where $H_{0,+}$ is the field at which the 0, + Landau subband passes the Fermi level, $\beta = \omega_c/\omega_e$, and the sum is carried out over all terms which have a nonnegative radicand.

The values of field at which the peaks and dips occur ($H_{l,\pm}$) and the corresponding values of $\Delta n_{l,\pm}$ are calculated by substituting the Fermi energy $\mu = l\hbar\omega_c \pm \frac{1}{2}\hbar\omega_e$ into the normalization integral $n_0 = n_- + n_+$. The results are

$$H_{l,\pm} = H_{0,+}[B_{l,\pm}(\beta)]^{-2/3}, \tag{12a}$$

$$\Delta n_{l,\pm} = n_0 A_{l,\pm}(\beta)/B_{l,\pm}(\beta), \tag{12b}$$

where

$$A_{l,\pm}(\beta) = \tfrac{1}{2}(1 \pm 1) \mp \sum_{m=1}^{l} [(m\beta)^{1/2} - (m\beta \pm 1)^{1/2}] \tag{12c}$$

and

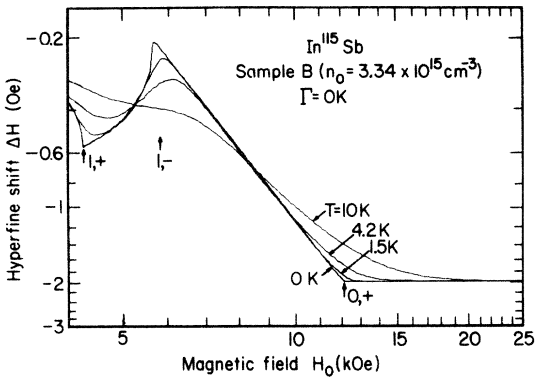

FIG. 8. Calculated hyperfine shift for n-type $In^{115}Sb$ in sample B ($n_0 = 3.34 \times 10^{15}$ cm^{-3}) as a function of magnetic field and temperature. The amplitudes of the OO decrease progressively as the temperature increases. Dingle broadening and band tailing have been excluded from these calculations. Saturation of ΔH is apparent at higher fields, and the region $\Delta H \propto H^3$ at $T = 0$ is clearly seen.

$$B_{l,\pm}(\beta) = \tfrac{1}{2}(1 \pm 1) + \sum_{m=1}^{l} [(m\beta)^{1/2} + (m\beta \pm 1)^{1/2}]. \tag{12d}$$

The terms in the sums are set equal to zero when $l = 0$ so $A_{0,\pm} = B_{0,\pm} = \frac{1}{2}(1 \pm 1)$ is independent of β. Values for $B_{l,\pm}(\beta)$ are tabulated up to $l = 3$ in BC[50] for $\beta = 2.8$. These results give the points at the extrema of the curves of ΔH vs H_0 for $T = 0$ shown in Figs. 8 and 9 for In^{115}. Values for $H_{0,+}$, $\Delta H_{0,+}$, and $H_{1,\pm}$ are tabulated in Table II. These values have been calculated from Eq. (12) using Eq. (7a) and the substitutions $\langle |u_F(0)|^2 \rangle^{115} = 9.35 \times 10^{25}$ cm^{-3} from the experiment of Gueron, [21] $\Omega = 0.68 \times 10^{-22}$

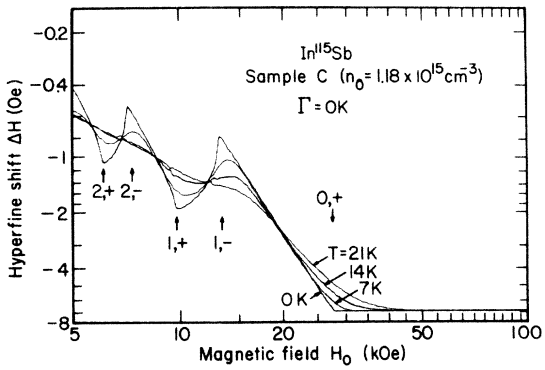

FIG. 9. Calculated hyperfine shift for n-type $In^{115}Sb$ in sample C ($n_0 = 1.18 \times 10^{16}$ cm^{-3}) as a function of magnetic field and temperature. The amplitudes of the OO decrease progressively as the temperature increases. Dingle broadening and band tailing have been excluded from these calculations. Saturation of ΔH is apparent at higher fields.

TABLE II. Calculated values[a] of $H_{0,+}$, $\Delta H_{0,+}$, $H_{1,-}$ and $H_{1,+}$ for $In^{115}Sb$ at $T=0$ K.

Sample	n_0 (10^{15} cm^{-3})	$H_{0,+}$ (kOe)	$\Delta H^{115}_{0,+}$ (kOe)	H_{1-} (kOe)	H_{1+} (kOe)
A	0.204	1.87	−0.101 (−0.190)	···	···
B	3.34	12.06	−1.650 (−1.967)	5.74	4.33
C	11.8	27.50	−5.829 (−6.950)	13.34	10.00

[a]Values of ΔH outside parentheses were calculated using Gueron's value (Ref. 21) $\langle |u_F(0)|^2\rangle^{115} = (9.35 \pm 1.0) \times 10^{25}$ cm^{-3}; values in parentheses are based on the best values obtained in this work, $\langle |u_F(0)|^2\rangle^{115}_{\text{expt}} = (11.15 \pm 0.80) \times 10^{25}$ cm^{-3}.

cm^{-3}, $\mu_B = 9.273 \times 10^{-21}$ erg/Oe, and the appropriate values of n_0 and β from Table I. Using these values in Eq. (7a) we find the calculated value of h,

$$h^{115}_{\text{calc}} = -\tfrac{8}{3}\pi \langle |u_F(0)|^2\rangle^{115} \Omega \mu_B = -0.494 \times 10^{-15} \text{ Oe cm}^3. \quad (13)$$

The experimental value h^{115}_{expt} [see Eq. (4)] is 19.3% larger than the calculated value, and implies that

$$\langle |u_F(0)|^2\rangle^{115}_{\text{expt}} = (11.15 \pm 0.80) \times 10^{25} \text{ cm}^{-3}. \quad (14)$$

Since this value of $\langle |u_F(0)|^2\rangle^{115}$ is consistent with our data, it will be used in all calculations here. It should be noted, however, that the difference between this value and Gueron's value is just within the combined experimental errors.

For magnetic fields in the range $H_{1,-} \le H \le H_{0,+}$, the explicit expressions for Δn and thus ΔH are found to be[51]

$$\Delta n/n_0 = \Delta H/\Delta H_{0,+} = (H/H_{0,+})^3, \quad (15)$$

where $\Delta H_{0,+}$ is the value of ΔH upon complete polarization of the conduction electrons. The experimental behavior of ΔH in sample C is seen from Figs. 5 and 6 to be approximately cubic in H_0 for fields above 16.5–17.0 kOe.

2. Nonzero temperatures

The effect of a finite temperature on the QO is to round off the peaks and decrease their amplitude. This can be visualized by referring to Fig. 7. As each Landau subband rises, its final stage of depopulation will begin when it gets within kT of the Fermi energy. It is this final stage of depopulation which is responsible for the sharpness of the QO peaks. Hence, at a finite temperature the peak is spread out over a range of field corresponding to a change of about kT in Fermi energy relative to the bottom of the subband.

To calculate the hyperfine shifts for $T \neq 0$ we will use the smallness parameter $\lambda = (kT/\hbar\omega_e)^{1/2}$ and several other variables:

$$\epsilon = (E - \tfrac{1}{2}\hbar\omega_e)/kT, \quad (16a)$$

$$\epsilon_{l,\pm} = \epsilon - l\beta/\lambda^2 + (1 \mp 1)/2\lambda^2, \quad (16b)$$

$$\eta = (\mu - \tfrac{1}{2}\hbar\omega_e)/kT, \quad (16c)$$

$$\eta_{l,\pm} = \eta - l\beta/\lambda^2 + (1 \mp 1)/2\lambda^2. \quad (16d)$$

Using these substitutions in Eq. (7c) and using Eqs. (9) and (10), we obtain for the spin-state populations

$$n_\pm = AH\sqrt{kT} \sum_l \int_{\epsilon_{l,\pm}=0}^{\infty} \frac{\epsilon_{l,\pm}^{-1/2}\, d\epsilon_{l,\pm}}{1 + e^{\epsilon_{l,\pm} - \eta_{l,\pm}}} = \tfrac{1}{2}\sqrt{\pi}\, n_0 (\lambda^3_{0,+}/\lambda^2) \sum_l \mathfrak{F}_{-1/2}(\eta_{l,\pm}), \quad (17a)$$

where $\lambda_{0,+} = (kT/|g^*|\mu_B H_{0,+})^{1/2}$ and $\mathfrak{F}_j(\eta)$ is the Fermi-Dirac integral[52]

$$\mathfrak{F}_j(\eta) = \frac{1}{\Gamma(j+1)} \int_0^\infty \frac{\epsilon^j\, d\epsilon}{1 + e^{\epsilon - \eta}}. \quad (17b)$$

To obtain values for Δn, Eq. (17a) is substituted into the normalization integral $n_0 = n_- + n_+$ to solve for η. This is in turn substituted back into $n_\pm$ to obtain Δn and hence ΔH. This has been done numerically for several temperatures for samples B and C and the results are shown in Figs. 8 and 9.

At the lower temperatures, thermal broadening of the QO is confined to the regions near the peaks and dips. They are decreased in amplitude and displaced toward higher fields. This, for example, is in contrast to the QO in $1/T_1$ and interband Faraday rotation where thermal smearing displaces the peaks toward lower fields.[5,6]

B. Nonthermal broadening of quantum oscillations

It is significant that the theoretical curves calculated for 4.2 and 7 K are found to be sharper than the experimental data for the lowest temperatures in samples B and C, respectively. It is to this discrepancy that we now turn our attention.

To explain the data it is necessary to include in the theory the effects of two mechanisms which broaden the electronic density of states. The two mechanisms are electron collisions with charged impurities (Dingle broadening) and the effects of spatial fluctuations in n_0 due to the random distribution of impurity ions (band tailing).

1. Dingle broadening

The effects of electron collisions with charged impurities were originally described for the de Haas–van Alphen (dHvA) effect by Dingle,[22] and a rigorous treatment has been given by Brailsford.[53] Kubo *et al.*[54] have given a detailed description of the effects of scattering on transport properties in the high field ($\hbar\omega_c \gg kT$) and quantum limit ($\hbar\omega_c$

$\gtrsim \mu$) regimes. One of the principal results of the papers of Dingle and Brailsford is that in the range of fields such that $\hbar\omega_c < kT$, the effects of collision broadening on the dHvA and Shubnikov-de Haas effects can be approximated in terms of an apparent increment in temperature called the Dingle temperature, $T_D = \hbar/2\pi k\tau$, where τ is the lifetime of the electron states.

In a sample without any impurities, the density of conduction-electron states is as discussed in Sec. IV A. This density of states represents a situation in which there are many sharp degenerate levels arranged in such a sequence that they produce the discontinuities seen in Fig. 7. If charged impurities are then added to the problem, new energy eigenstates and levels will occur. Although these states will also be sharp, their distribution in energy will not be the same as for the system without impurities. From the viewpoint of a perturbation treatment, one considers the impurities as a perturbation which splits and/or "lifetime broadens" the originally unperturbed states. This leads to a smearing of the unperturbed density of states, which is taken to approximate the exact density of states which includes the effect of impurities.

For problems involving thermal averages over many states, the effect of impurities in determining the exact density of states can often be replaced by using the original sharp density of states and a thermal distribution function characterized by a higher fictitious temperature; i.e., the smearing of the density of states by impurities can be approximated by an equivalent thermal smearing.

Although the concept of a Dingle temperature is not strictly valid in the range of fields studied in this work, it is the only simple method to include scattering, and we will discuss it from that point of view. The broadened QO curves can be seen by referring to Figs. 8 and 9 where the effects of temperatures up to 21 K are shown. It is important to remember that these curves are calculated strictly for thermal broadening and apply to collision broadening only to the extent that such comparison is valid. The Dingle temperatures and the corresponding effective temperatures ($T^* = T + T_D$) which best fit our data are shown in Table III along with the corresponding lifetimes. It has been assumed here that no other broadening mechanisms are operative.

In calculating the hyperfine shift we will proceed on the assumption that the time of interest is given by $\tau = \hbar/\Delta E$, where ΔE is the width of the broadened energy levels. The lifetime has been calculated by Robinson and Rodriguez in the limit of low magnetic fields.[55] Theoretical values of the Dingle temperatures calculated from their results applied to InSb are shown in Table III. Also shown are values for sample B at $H = H_{0,+}$ calculated from the results of several workers.[56–58] The results of Kawabata and of Kawamura *et al.* are transport relaxation times and differ from the energy level lifetimes by a multiplicative factor. This factor has been calculated by Brailsford and is included in the values shown in the table. Ciobanu and Bányai[58] have derived a relationship between the lifetime for $H = 0$ and that for $H > H_{0,+}$. These results have been applied to the results of Robinson and Rodriguez to obtain the values in the last column of the table.

Calculation of the lifetime for fields less than $H_{0,+}$ appears to be quite complex and has not been done here.

2. *Band tailing*

The effects of spatial fluctuations of the impurity density in semiconductors have been studied theoretically and experimentally for $H = 0$, and for high magnetic fields.[23,34,59–72] We will use the following

TABLE III. Experimental and theoretical values for the Dingle temperature (T_D) and the effective temperature ($T^* = T + T_D$).

Sample	Lattice temperature T (K)	Effective temperature T^* [a] (K)	Dingle temperature T_D(expt.) (K)	Lifetime $\tau_{expt} = \frac{\hbar}{2\pi k T_D}$ (10^{-13} sec)	T_D(theor.)[b] (K)	T_D(theor.)[c] at $H = H_{0,+}$ (K)	T_D(theor.)[d] at $H = H_{0,+}$ (K)
B	1.5	8 ± 3	6.5 ± 3	1.9 ± 1	2.2	6.1	55.6
B	4.2	5 ± 1	0.8 ± 0.8	15 ± 15	2.2	6.1	55.6
C	0.4	14 ± 3	13.6 ± 3	0.89 ± 0.20	3.5	···	···
C	1.5	14 ± 3	12.5 ± 3	0.97 ± 0.23	3.5	···	···

[a]These values of T^* are the best fits to our data with the assumption that Dingle broadening is the only operative broadening mechanism.

[b]These values are obtained with the low-field theory of Ref. 55.

[c]Obtained from the theory of Refs. 53, 56, and 57.

[d]These values are obtained from the results of Ref. 58 applied to the low-field values in column 6.

conventional model to discuss these effects. Because of the random distribution of donor ions, there are spatial density fluctuations which cause fluctuations in the electronic potential energy. Within a volume defined roughly by the electrostatic screening length, the potential will vary slowly and can be taken approximately as constant. Inside this volume there exists a density of states which reflects the local impurity concentration, and which changes from one volume to the next. By averaging over all such volumes in the sample, one obtains the total density of states. This average can be taken by averaging the local density of states over an appropriate distribution function. This function will be a Gaussian distribution when the screening radius is large enough so that the average number of ions within the screening volume is large.[64] Although this condition is not strictly met in our experiments, we shall nevertheless use a Gaussian distribution, as it is easy to use and should lead to qualitatively correct results. This averaging results in a density of states which is broadened and has Gaussian-like tails at the bottom of each Landau subband.

One point that should be noted is that the conduction-electron wave-function amplitudes peak up in the vicinity of the donor ions and sag down far away from them. Thus, even if the ions are uniformly distributed throughout the crystal, for each electron in a given energy level there will be a spatial variation of $\langle |u_F(0)|^2 \rangle$, and hence in the hyperfine shift. This variation will broaden the NMR lines.[73] In the experiments described here this effect is small compared to the In^{115} linewidth (9 Oe) and was not observed.

The quantity which characterizes the width of the broadening is the rms of the spatial fluctuations of the electronic potential energy (the flucuation potential Γ):

$$\Gamma = 2\pi^{1/2}(e^2/\kappa\lambda_s)(N\lambda_s^3)^{1/2}, \tag{18}$$

where κ is the dielectric constant (16.6 for InSb), λ_s is the screening length, and N is the total impurity concentration. The band-tailing theory in high magnetic fields was developed by Dyakonov, Efros, and Mitchell[23] (hereafter referred to as DEM) for highly compensated semiconductors. However, it also applies to uncompensated semiconductors, where it causes a nearly rigid downward shift of the entire conduction band.[59] Such a shift, of course, has no effect on the QO. Thus the DEM results are used here without modification.

In applying the results of DEM to the hyperfine shift we ignore the effects of fluctuations on the effective mass and g factor. We also ignore any possible dependence of the fluctuation potential on the magnetic field.

The density of states for a given spin and Landau level is (DEM)

$$g_{l,\pm}(E,\Gamma) = (AH/\sqrt{\Gamma})\,G(kT\epsilon_{l,\pm}/\Gamma), \tag{19a}$$

where

$$G(x) = \frac{1}{\sqrt{\pi}} \int_{-\infty}^{x} \frac{e^{-y^2}}{(x-y)^{1/2}}\,dy\,. \tag{19b}$$

By summing over l as in Eq. (10) we obtain the full density of states for each spin state. Substituting Eq. (19) into Eq. (7c) we obtain, after reversing the order of integration,

$$n_{\pm}(\Gamma) = AH\left(\frac{kT}{\pi}\right)^{1/2} \sum_l \int_{-\infty}^{\infty} dy \int_{\Gamma y/kT}^{\infty} d\epsilon_{l,\pm} \times \frac{(\epsilon_{l,\pm} - \Gamma y/kT)^{1/2} e^{-y^2}}{1 + e^{\epsilon_{l,\pm} - \eta_{l,\pm}}} = \frac{n_0\lambda_{0,\pm}^3}{2\lambda^2} \sum_l \int_{-\infty}^{\infty} \mathfrak{F}_{-1/2}(\eta_{l,\pm} - \Gamma y/kT) e^{-y^2} dy\,. \tag{20}$$

This can be compared with the results for the unbroadened case [Eq. (17a)].

Rearranging terms in Eq. (20) we get

$$n_{\pm}(\Gamma) = \frac{1}{\sqrt{\pi}} \int_{-\infty}^{\infty} \tilde{n}_{\pm}(\eta - \Gamma y/kT) e^{-y^2} dy\,, \tag{21}$$

where $\tilde{n}_{\pm}(\eta - \Gamma y/kT)$ is the population of electrons in each spin state if there were no band tailing.

Equation (21) is substituted into the normalization integral to solve for η, which is then used to calculate Δn and ΔH. We have done this numerically using several values of Γ, for samples B and C at temperatures of 1.5 and 0.4 K, respectively. The results are displayed in Figs. 10 and 11.

At lower fields the QO are completely smoothed out for the larger values of Γ. The QO begin to

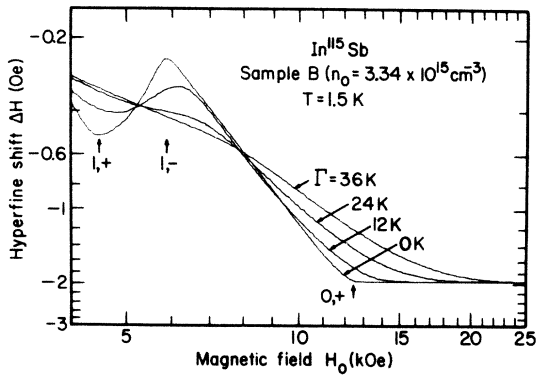

FIG. 10. Calculated hyperfine shift for n-type $In^{115}Sb$ as a function of magnetic field for sample B ($n_0 = 3.34 \times 10^{15}$ cm^{-3}) at $T = 1.5$ K. The calculations include band tailing for several values of the fluctuation potential (Γ). The QO amplitudes are decreased progressively as Γ increases. Saturation of ΔH is apparent at higher fields.

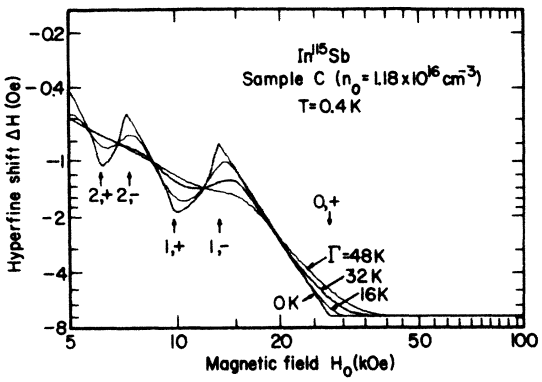

FIG. 11. Calculated hyperfine shift for n-type $In^{115}Sb$ as a function of magnetic field for sample C ($n_0 = 1.18 \times 10^{16}$ cm^{-3}) at $T = 0.4$ K. The calculations include band tailing for several values of the flucatuation potential (Γ). The amplitudes of the QO decrease progressively as Γ is increased. Saturation of ΔH is apparent at higher fields.

appear at magnetic fields such that

$$\hbar\omega_c \gtrsim \Gamma, \tag{22}$$

which is a more stringent condition for the importance of the magnetic field than that given by DEM ($\hbar\omega_c \gtrsim \Gamma$). This is not surprising, however, since the hyperfine shift depends on the difference of the populations of the two electronic spin states.

The theoretical curves with band tailing have also been plotted over the experimental data for samples B and C (Figs. 3–6). The temperatures used in these plots were the actual sample temperatures, and the values of Γ were those which gave reasonably good agreement with the data by assuming that all nonthermal broadening is due to band tailing. These values are given in Table IV with their corresponding screening lengths calculated from Eq. (18). Also given are several theoretical values for Γ and their respective screening radii, along with similar values for the InSb sample used by Kaufman and Neuringer.[34]

The values of Γ calculated for the nondegenerate case have been included only for comparison since, in samples B and C, the electrons are degenerate for all temperatures and magnetic fields used in these experiments.

It can be seen from Table IV that the theoretical values using the zero-field Fermi-Thomas screening radius are too large by as much as 100%. One possible explanation is that quantum effects of the large magnetic field are not properly accounted for in such a calculation.[74] Another possibility is that the Fermi-Thomas length is not the appropriate one to be used in calculating Γ. A more detailed theoretical analysis is necessary if this question is to be resolved, especially since experiments in the magnetic freeze-out regime yield results which tend to agree with the theory.[34,72]

3. *Comparison of Dingle broadening with band tailing*

Up to this point we have been discussing each nonthermal broadening mechanism without reference to the other. However, it can be seen from Figs. 8–11 that the effects of each mechanism taken separately yields very similar results. In fact, the differences between the types of broadening are too small to measure experimentally.

Since in our experiments the two mechanisms are probably active simultaneously, a calculation has been performed for an intermediate combination of Γ and T^* which will result in hyperfine shift QO which are broadened to the same extent as the experimental results. This curve is plotted

TABLE IV. Experimental and theoretical values of Γ and λ_s.

Sample	Temperature (K)	Γ(expt.)[a] (K)	λ_s(expt.)[b] (Å)	Γ(theor.)[c] Fermi-Thomas (K)	λ_s(theor.)[c] Fermi-Thomas (Å)	Γ(theor.)[d] nondegenerate (K)	λ_s(theor.)[d] Non degenerate (Å)
B	1.5	18 ± 6	76 ± 50	37	325	16	60
B	4.2	7 ± 5	12 ± 12	37	325	21	100
C	0.4	32 ± 6	66 ± 25	61	246	15	16
C	1.5	32 ± 6	66 ± 25	61	246	21	32
KN[e]	0.8	8.1	26	30	356	12	56

[a]These values of Γ(expt.) are the best fits to our data with the assumption that band tailing is the only operative braodening mechansim.

[b]Obtained with Γ(expt.) and Eq. (18).

[c]Calculated from $\lambda_s = (\kappa\mu/6\pi n_0 e^2)^{1/2}$, the Fermi-Thomas screening length at $H = 0$, and Eq. (18).

[d]Calculated from $\lambda_s = (\kappa kT/4\pi n_0 e^2)^{1/2}$, the nondegenerate screening length at $H = 0$, and Eq. (18).

[e]Data of Ref. 34; $n_0 = 2 \times 10^{15}$ cm^{-3}.

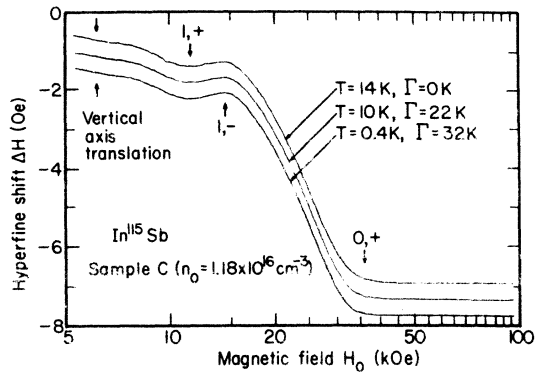

FIG. 12. Comparison of the effects on ΔH of band tailing with thermal smearing and/or Dingle broadening. Several plots using different combinations of both effects but giving similar results are shown. Parameters characteristic of sample C ($n_0 = 1.18 \times 10^{16}$ cm^{-3}) have been used. The two lower curves have been displaced vertically for clarity. It is seen that all three curves are nearly indistinguishable.

in Fig. 12 for $T = 10$ K, $\Gamma = 22$ K along with two of the previous curves for sample C ($T = 14$ K, $\Gamma = 0$ K and $T = 0.4$ K, $\Gamma = 32$ K). The curves have been translated vertically to make them easier to see.

It is probably useful to note that the numerical solutions for many different combinations of Γ and T^*, all of which produce an equal amount of broadening, result in the following empirical relationship:

$$(\Gamma/\Gamma_0)^2 + (T^*/T_0^*)^2 = 1. \tag{23}$$

Here, Γ_0 is the value of Γ which produces the required broadening when $T^* = 0$, and T_0^* is similarly defined. The values of Γ_0 and T_0^* appropriate to our data are shown in Table V along with the experimental values of Γ and T^*. It is interesting to note that the ratio Γ_0/T_0^* is always in the range 2.3–2.4. This is a consequence of the requirement that both T_0^* and Γ_0 produce the same amount of broadening, and the fact that the width of the derivative of the Fermi-Dirac distribution is about $3kT$.

There does not appear to be, at present, any way to satisfactorily separate out the contributions of the two broadening mechanisms by using our data for the hyperfine shift. However, the results of Robinson and Rodriguez have been used in an attempt to make such a separation.[55] The resulting values for sample C are $T_D = 3.5$ K, $\Gamma = 31$ K. These results are included in the last column of Table V. It is apparent from the results of these calculations that the hyperfine shift oscillations are insensitive to the details of the actual broadening mechanisms, and that such information is more readily obtained by other methods.[34,68–72]

C. Type-A and type-B peaks

In their measurements, BC observed two additional peaks in $1/T_1$ at fields higher than those at which the last QO occurs.

The first peak (type-A) was observed in their data for several samples including sample B at 1.3 K and 16 kOe. This peak was fairly broad, extending from about 12 kOe to above 20 kOe. One of the proposed explanations is based on a model of a narrow impurity band, split off from the bottom of the 0, + Landau subband, but which lies above the bottom of the 0, − subband.[75] As H_0 varies and the Fermi level moves through the impurity band in the density of states, the relaxation rate will rise to a maximum, and then drop back down again. It has been shown that, to agree with the experiments of BC, up to 8% of n_0 must be in this impurity band.[76] If this were the case, one would expect an increase of 8% in the magnitude of ΔH as the field increases and μ passes through this impurity band. For sample B, this would amount to an increase of about 0.16 Oe. This increment of ΔH is just under the experimental resolution of our data at 1.5 K. However, at 4.2 K, the data show sufficient resolution that such a change would just be observable. At this temperature the $1/T_1$ peak is expected to start at about 14 kOe and reach a maximum at 18–19 kOe. It

TABLE V. Comparison of the effective temperature and the fluctuation potential.

Sample	Temperature (K)	Γ(expt.)[a] (K)	T^*(expt.)[a] (K)	Γ_0[b] (K)	T_0^*[b] (K)	Γ_0/T_0^*	Γ(theor.)[c] (K)
B	1.5	18	8	18.3	7.8	2.35	23
B	4.2	7	5	12.1	5.1	2.37	7.2
C	0.4–1.5	32	14	32	14	2.29	31

[a]The values of Γ(expt.) and T^*(expt.) are the best fits to our data with the assumption that each is, in turn, the only operative broadening mechanism.

[b]See Sec. IV B 3.

[c]These values calculated from Eq. (23) using theoretical values for T_D calculated from Ref. 55.

can be seen from Fig. 4 that there is no obvious variation in ΔH corresponding to the type-A peaks in $1/T_1$ at this temperature. Further work at high fields and lower temperatures is necessary before any definite statements can be made with regard to the origin of the type-A phenomenon.

A type-B peak in $1/T_1$ in sample A occurs around 14 kOe and 1.4 K. At 4.2 K this peak occurs just above 20 kOe. The relaxation rate at 1.4 K begins to rise toward the peak as the field is increased above 8 kOe; the corresponding field for $T=4.2$ K is 10 kOe. Bridges and Clark suggest that the origin of this peak in $1/T_1$ is magnetic freeze-out of electrons from the conduction band, which has been observed to occur in this region of field and electron concentration.

It is natural to consider the possibility that a corresponding effect might be seen in the hyperfine shift.

If the Fermi level lies below the bound state which splits off from the 0, + subband when freeze-out occurs, then as the electronic wave functions shrink in volume, the average value of ΔH will not change since the wave functions must always be normalized. Furthermore, one would expect to see an increase in the NMR linewidths due to the distribution of hyperfine shifts.[73]

For the range of fields for which freeze-out occurs in sample A, the Fermi level is expected to be below the bound state which lies below the 0, + subband.[30,75,76] One would thus not expect to see any change in ΔH in this regime for sample A. In cases where the (+) bound state lies below the Fermi level, one would expect to see an increase in the magnitude of ΔH as H_0 is increased as discussed above with regard to the type-A phenomenon.

From Figs. 1 and 2 it is seen that, within experimental resolution, there is no change in ΔH corresponding to the occurrence of magnetic freeze-out. This null result is as expected, since for this sample $\Delta H^{115}_{0,+}$ is only -0.12 Oe and any decrease in its magnitude would be too small to resolve.

V. CONCLUSIONS

We have measured the Knight shift of In^{115} and Sb^{121} in InSb with respect to $In_2(SO_4)_3$ and $HSbF_6$ as a function of magnetic field between 4.2 and 0.4 K. The observed shifts are resolved into the chemical shift and the hyperfine shift due to the conduction electrons.

The main feature of these measurements is the observation of the quantum oscillations whose positions agree very well with the theoretical predictions.

It is necessary to consider nonthermal broadening to explain the data. Two such mechanisms are included here. The first mechanism was the broadening of the electronic density of states due to electron collisions with charged impurities (Dingle broadening). This effect was approximated by treating it as an added increment of thermal smearing given by the Dingle temperature (T_D). The second mechanism is the spatial fluctuations of the electron concentration caused by the random distribution of impurities in the crystal (band tailing). This effect is included by using the theory of DEM[23] which gives a broadened density of states with Gaussian-like tails.

Both mechanisms, either separately or in combination, give results which are in good agreement with experiment. The differences between ΔH-vs-H_0 curves calculated on the basis of each mechanism would not be experimentally observable in InSb.

The two broadening mechanisms are found to be related in that for a given amount of broadening of the QO, the effective temperature ($T^* = T + T_D$) and the fluctuation potential (Γ) are related by the empirical relationship

$$(\Gamma/\Gamma_0)^2 + (T^*/T_0^*)^2 = 1,$$

where Γ_0 and T_0^* are the values of Γ and T^* which give the full amount of broadening of the QO when each is used alone in the calculations.

Theoretical estimates for T_D using existing theories for electron state lifetimes are consistent with our experimental data. However, a more complete theoretical picture is necessary before it can be told whether this agreement is meaningful or fortuitous.

Theoretical calculations of Γ using the Fermi-Thomas screening radius are nearly twice as large as the maximum values allowed by our data. Further theoretical analysis of the problem is necessary to properly calculate values for the fluctuation potential.

Within our experimental resolution, no variations in H were observed at fields which correspond to the type-A and type-B peaks observed in the $1/T_1$ data of BC. A variation of ΔH due to an impurity band containing enough electrons to explain the type-A peak in $1/T_1$ should have been observable. It appears that, all things considered, impurity banding is an unlikely candidate as the origin of the type-A peaks.

With regard to the occurrence of the type-B peak, which coincides with magnetic freeze-out, no changes in ΔH were expected and none were observed. In the event that such changes were expected, due to the low concentration of sample A any such variations would be too small to be resolved experimentally.

Further experiments extending the range of fields and temperatures covered here would shed more light on the type-A and type-B phenomena

and perhaps allow a separation of the Dingle-broadening and band-tailing contributions to the observed nonthermal broadening.

ACKNOWLEDGMENTS

We thank G. Feher and R. A. Isaacson for providing the samples used in this work, and are grateful to F. Bridges for his comments. In addition, one of us (W. G. C.) would like to thank the Aspen Center for Physics for its hospitality while part of the manuscript was being prepared.

---

*Work supported in part by the Air Force Office of Scientific Research Grant No. 68-1528 and the National Science Foundation Grant No. GP 29878.

†Work performed in partial fulfillment of the requirements for the Ph.D. degree.

‡Present address: Los Alamos Scientific Laboratory, Los Alamos, N. M. 87544.

§Present address: Fachbereich Physik, Universität Konstanz, West Germany.

[1]R. J. Sladek, E. R. Gertner, and D. G. Seiler, Phys. Rev. B **3,** 2608 (1971); W. R. Wampler and M. Springford, J. Phys. C **5,** 2345 (1972).

[2]S. T. Pavlov, R. V. Parfen'ev, Yu. A. Firsov, and S. S. Shalyt, Zh. Eksp. Teor. Fiz. **48,** 1565 (1965) [Sov. Phys.-JETP **21,** 1049 (1965)].

[3]R. A. Isaacson and F. Bridges, Solid State Commun. **4,** 635 (1966).

[4]O. Beckman, E. Hanamura, and L. J. Neuringer, Phys. Rev. Lett. **18,** 773 (1967).

[5]F. Bridges and W. G. Clark, Phys. Rev. **182,** 463 (1969). This paper is referred to in the text as BC.

[6]R. B. Dennis, S. D. Smith, and C. J. Summers, Proc. R. Soc. A **321,** 303 (1971).

[7]T. P. Das and E. H. Sondheimer, Philos. Mag. **5,** 529 (1960).

[8]M. J. Stephen, Phys. Rev. **123,** 126 (1961).

[9]J. I. Kaplan, J. Phys. Chem. Solids **23,** 826 (1962).

[10]S. Rodriguez, Phys. Lett. **4,** 306 (1963).

[11]D. G. Dolgopolov and P. S. Bystrik, Zh. Eksp. Teor. Fiz. **46,** 593 (1964) [Sov. Phys.-JETP **19,** 404 (1964)].

[12]A. K. Zvezdin and P. S. Zyranov, Fiz. Met. Metalloved. **18,** 487 (1964) [Phys. Met. Metallogr. **18,** 7 (1964)].

[13]M. L. Glasser, Phys. Rev. **150,** 234 (1966).

[14]D. A. Zhogolev and D. G. Dolgopolov, Fiz. Tverd. Tela **9,** 1256 (1967) [Sov. Phys.-Solid State **9,** 982 (1967)].

[15]J. M. Reynolds, R. G. Goodrich, and S. A. Khan, Phys. Rev. Lett. **16,** 609 (1966).

[16]S. A. Khan, R. G. Goodrich, and J. M. Reynolds, Bull. Am. Phys. Soc. **12,** 184 (1967); S. A. Khan, J. M. Reynolds, and R. G. Goodrich, Phys. Rev. **163,** 579 (1967).

[17]H. R. Khan, J. M. Reynolds, and R. G. Goodrich, Phys. Rev. B **2,** 4796 (1970); R. G. Goodrich, S. A. Khan, and J. M. Reynolds, Phys. Rev. B **3,** 2379 (1971).

[18]A. Willig and B. Sapoval, Solid State Commun. **11,** 1077 (1972).

[19]A. Abragam, *The Principles of Nuclear Magnetism* (Clarendon, Oxford, England, 1962), pp. 175 and 203.

[20]Reference 19, p. 200.

[21]M. Gueron, Phys. Rev. **135,** A200 (1964).

[22]R. B. Dingle, Proc. R. Soc. A **211,** 517 (1952).

[23]M. I. Dyakonov, A. L. Efros, and D. L. Mitchell, Phys. Rev. **180,** 813 (1969). This paper is referred to in the text as DEM.

[24]R. A. Isaacson, Phys. Rev. **169,** 312 (1963).

[25]F. Bridges and W. G. Clark, Phys. Rev. **164,** 288 (1967).

[26]W. G. Clark and R. A. Isaacson, J. Appl. Phys. **38,** 2284 (1967).

[27]Y. Yafet, R. W. Keyes, and E. N. Adams, J. Phys. Chem. Solids **1,** 137 (1956).

[28]R. W. Keyes and R. J. Sladek, J. Phys. Chem. Solids **1,** 143 (1956).

[29]H. P. R. Frederikse and W. R. Hosler, Phys. Rev. **108,** 1136 (1957).

[30]R. J. Sladek, J. Phys. Chem. Solids **5,** 157 (1958).

[31]R. J. Sladek, J. Phys. Chem. Solids **8,** 515 (1959).

[32]J. Haslett and W. Love, J. Phys. Chem. 8, 518 (1959).

[33]E. H. Putley, J. Phys. Chem. Solids **22,** 241 (1961).

[34]L. A. Kaufman and L.J. Neuringer, Phys. Rev. B **2,** 1840 (1970).

[35]G. A. Miranda, Ph.D. thesis (University of California, Los Angeles, 1972) (unpublished).

[36]Our observed ratio ν_{115}/ν_{79} was 0.874 548 $\pm$ 0.000 004 for a dilute aqueous solution of $In_2(SO_4)_3$. The ratio $\nu_{121}/\nu_{79} = 0.955\,180 \pm 0.000\,026$ was determined from our value for ν_{115}/ν_{79} and the values for ν_x/ν_D contained in W. W. Warren, Jr. and W. G. Clark, Phys. Rev. **177,** 600 (1969).

[37]J. Itoh and Y. Yamagata, J. Phys. Soc. Jap. **13,** 1232 (1958).

[38]Y. Yafet, J. Phys. Chem. Solids **21,** 99 (1961).

[39]J. S. Blakemore, *Semiconductor Statistics* (Pergamon, New York, 1962); Chaps. 1 and 2 contain a discussion of the density of states of a free electron under a high magnetic field.

[40]E. H. Johnson and D. H. Dickey, Phys. Rev. B **1,** 2676 (1970).

[41]G. Bemski, Phys. Rev. Lett. **4,** 62 (1960).

[42]L. Roth, B. Lax, and S. Zwerdling, Phys. Rev. **114,** 90 (1959).

[43]F. Kessler and E. Sutter, Z. Naturforsch. A **16,** 1173 (1961).

[44]H. Ehrenreich, J. Phys. Chem. Solids **2,** 131 (1957).

[45]E. O. Kane, J. Phys. Chem. Solids **1,** 249 (1957).

[46]E. Burstein, G. Picus, and H. Gebbie, Phys. Rev. **103,** 825 (1956).

[47]B. Lax, J. G. Mavroides, H. J. Zeiger, and R. J. Keyes, Phys. Rev. **122,** 31 (1961).

[48]B. D. McCombe and R. J. Wagner, Phys. Rev. B **4,** 1285 (1971).

[49]This approximation is probably valid since the conduction electrons occupy less than 10^{-6} of the volume of the k space.

[50]Reference 5. There is an error in Table II that should be noted. The expression for $B_{2,-}(\beta)$ should read $\beta^{1/2} + (2\beta)^{1/2} + (\beta - 1)^{1/2} + (2\beta - 1)^{1/2}$.

[51]D. A. Zhogolev, Fiz. Tverd. Tela **11,** 50 (1969) [Sov. Phys.-Solid State **11,** 37 (1969)].

[52]Reference 39, Appendixes B and C.

[53]A. D. Brailsford, Phys. Rev. **149,** 456 (1966).

[54]R. Kubo, S. Miyake, and N. Hashitsume, *Solid State Physics*, edited by F. Seitz and D. Turnbull (Academic, New York, 1965), Vol. 17, p. 269.

[55]J. E. Robinson and S. Rodriguez, Phys. Rev. **135,** A779 (1964); Phys. Rev. **137,** A663 (1965).

[56]H. Kawamura, H. Saji, M. Fukai, K. Sekido, and I. Imai, J. Phys. Soc. Jap. **19,** 288 (1964).

[57]A. Kawabata, J. Phys. Soc. Jap. **23,** 999 (1967).

[58]G. Ciobanu and L. Bányai, Phys. Status Solidi **3,** 2299 (1963).

[59]P. A. Wolff, Phys. Rev. 126, 405 (1962).

[60]V. L. Bonch-Bruevich, Fiz. Tverd. Tela **4,** 2660 (1962) [Sov. Phys.-Solid State **4,** 1953 (1963)].

[61]V. L. Bonch-Bruevich, Fiz. Tverd. Tela **5,** 1852 (1963) [Sov. Phys.-Solid State **5,** 1353 (1964)].

[62]E. G. Tsitsishvili, Fiz. Tverd. Tela **8,** 1193 (1966) [Sov. Phys.-Solid State **8,** 950 (1966)].

[63]B. I. Halperin and M. Lax, Phys. Rev. **148,** 722 (1966).

[64]M. Lax and B. I. Halperin, J. Phys. Soc. Jap. Suppl. **21,** XXX (1966).

[65]T. Lukes, K. T. S. Somaratna, and K. Tharmalingam, J. Phys. C **3,** 1631 (1970).

[66]A. L. Efros, Zh. Eksp. Teor. Fiz. **59,** 880 (1970) [Sov.

Phys.-JETP **32,** 479 (1971)].
[67]H. Ikoma, J. Phys. Soc. Jap. **30,** 1509 (1971).
[68]E. O. Kane, Phys. Rev. 131, 79 (1963).
[69]L. V. Keldysh and G. P. Proshko, Fiz. Tverd. Tela **5,** 2481 (1964) [Sov. Phys.-Solid State **5,** 2481 (1964)].
[70]A. Mooradian and H. Y. Fan, Phys. Rev. **148,** 873 (1966).
[71]M. I. Dyakonov, A. L. Efros, and D. L. Mitchell, Phys. Rev. **180,** 819 (1969).
[72]T. O. Poehler, Phys. Rev. B **4,** 1223 (1971).
[73]G. Feher, Phys. Rev. **114,** 1219 (1959); R. K. Sundfors and D. F. Holcomb, Phys. Rev. **136,** A810 (1964).
[74]D. Redfield and M. A. Afrimowitz, Philos. Mag. **19,** 831 (1969).
[75]G. Benford and N. Rostoker, Solid State Commun. **6,** 705 (1968).
[76]G. Benford, Ph.D. thesis (University of California, San Diego, 1967) (unpublished).